Processing and Application of Ceramics 11 [2] (2017) 160–169
https://doi.org/10.2298/PAC1702160M

Influence of starting powder milling on magnetic properties of Mn-Zn ferrite

Miodrag M. Milutinov[1,*], Maria Vesna Nikolić[2], Snežana G. Luković[1], Nelu Blaž[1], Nebojša Labus[3], Obrad S. Aleksić[2], Ljiljana D. Živanov[1]

[1]*Faculty of Technical Sciences, University of Novi Sad, Trg Dositeja Obradovica 6, 21000 Novi Sad, Serbia*
[2]*Institute for Multidisciplinary Research, University of Belgrade, Kneza Višeslava 1, 11030 Beograd, Serbia*
[3]*Institute of Technical Sciences of SASA, Knez Mihailova 35, 11000 Beograd, Serbia*

Received 13 February 2017; Received in revised form 9 June 2017; Accepted 19 June 2017

Abstract

In this paper, the influence of additional sieving and milling of starting industrial Mn-Zn powders on magnetic properties was investigated. The starting powder was milled for 60 minutes, followed by sieving through 325 and 400 meshes. The starting and milled powders were used to fabricate toroid shaped samples sintered at 1200 °C for 2 hours. Structural parameters of the fabricated samples were analysed by X-ray diffraction and scanning electron microscopy. Complex permeability, core loss density, and hysteresis were measured using the modified watt-meter method. The complex permeability and hysteresis loop were modelled with a new model proposed in the paper. The core loss density was modelled with the Steinmetz empirical equation. The experimental results and calculations show the significance of the additional milling and sieving process on magnetic properties of Mn-Zn ferrite in the frequency range 0.1–10 MHz. These processes increase the relative permeability about 3 times and decrease the core loss 4 times by milling of the starting powder.

Keywords: *ferrites, milling, sieving, structural characterization, magnetic properties*

I. Introduction

Magnetic properties of Mn-Zn ferrites are mainly determined by their chemical compositions and microstructures that are very sensitive to the method of powder preparation and sintering process. The sintered density and grain size of the starting ferrite material have been revealed to be crucial factors for obtaining desired magnetic properties [1–4]. The grain size of starting powders can be reduced by milling process resulting in increased permeability and saturation [5–7]. Both low and too high sintering temperatures degrade magnetic properties and optimal conditions are necessary to obtain the best results [8,9].

Our previous investigation presented the influence of starting powder milling on electrical properties of Mn-Zn ferrite [10]. Therefore, we decided to investigate the influence of starting powder sieving and milling on the core loss density of Mn-Zn ferrite with similar composition used in our previous paper [10]. The complex permeability, core loss density and hysteresis loop of the sintered samples were measured using a modified watt-meter measurement technique adjusted to the low-input-impedance digital storage oscilloscope [11]. The measured magnetic properties were additionally modelled.

*Corresponding author: tel: +381 21 4852577,
e-mail: *miodragm@uns.ac.rs*

II. Experimental procedure

2.1. Sample preparation

The influence of starting powder sieving and milling on magnetic properties of Mn-Zn ferrite was analysed by comparing the magnetic properties of four toroidal samples. These samples were fabricated using starting industrial powder, which was additionally processed, milled and sieved.

The industrial powder (M-30, IHIS Ferrites RS), used as the starting Mn-Zn powder, has the following composition $Mn_{0.63}Zn_{0.37}Fe_2O_4$ 93 wt.% with 7 wt.% excess Fe_2O_3 (it is denoted as MZ-0). This powder was used to obtain three different powders denoted MZ-1, MZ-1-325, and MZ-24-400 (Table 1). The powder MZ-1 was obtained from the starting MZ-0 powder

Table 1. Powders used for the sample preparation

Sample	Powder	Milling duration [hour]	Sieve mesh dimension
A	MZ-0	0	Not sieved
B	MZ-1	1	Not sieved
C	MZ-1-325	1	325
D	MZ-24-400	24	400

by milling for 1 h in a planetary ball mill. The powder MZ-1-325 was obtained from the powder MZ-0 by milling in a planetary ball mill for 1 h and then sieving through a 325 mesh (sieve size ~45 μm). The powder MZ-24-400 was derived from the powder MZ-1 by additional milling in mortar grinder (Fritsch Pulverisette type 02.102) for 24 h and sieving through a 400 mesh (sieve size ~38 μm).

These four powders (MZ-0, MZ-1, MZ-1-325 and MZ-24-400) were used to obtain toroid shaped samples A, B, C, and D, respectively, with an average outer diameter of 9.8 mm, inner diameter of 4.3 mm and height of 2.5 mm. Toroid samples were obtained using a specially made tool/mould for such a shape and compacted with applied uniaxial pressure of 200 MPa on both sides without binder and lubricant. All samples were sintered at 1200 °C for 2 h with a heating rate of 10 °C/min and natural cooling.

2.2. Measurement method

Magnetic properties of the toroid shaped samples (Core under test – CUT) were measured using an HP3314A signal generator and a DSO90604A digital storage oscilloscope (DSO). The signal generator has the frequency range from DC to 20 MHz and the amplitude range from 0.01 mV_{pp} to 30 V_{pp}. The DSO is a high-performance oscilloscope from Keysight Technology®, with a 6 GHz analogues bandwidth, 20 GSa/s sampling rate, and four 50 Ω-input impedance channels. The measurement setup is shown in Fig. 1, which is modified classic watt-meter technique. Due to the low input impedance of used oscilloscope, the classic wattmeter method is modified by adding two new resistors R_2 and R_3 connected in series to increase the net resistance in the secondary winding.

The DSO with the sensitivity of 1 mV/div and maximum input voltage ±5 V ensures a 74 dB measurement range. The voltage divider located in the secondary winding does not reduce the measurement range. Instead, it shifts the lower and upper limit of the measurement range. The resistances of modified wattmeter method are adjusted to the low input impedance digital storage oscilloscope and Mn-Zn operating frequency range, as described in [11].

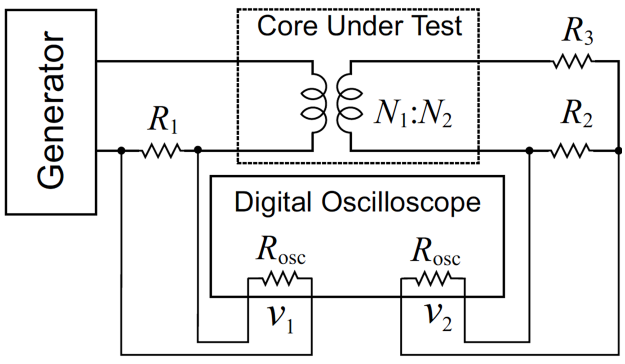

Figure 1. Measurement setup for the two-winding wattmeter method, based on a DSO90604A digital oscilloscope with 50 Ω-input impedance channels

III. Results

Our intention was to investigate how the milling and/or sieving of the commercial powder change its magnetic properties. The influence of the milling and/or sieving is analysed by comparing the complex permeability, core loss density and hysteresis loop of the starting powder (sample A) with the milled powders (samples B-D).

3.1. Structural characterization

The average sample density was determined as 4.84, 4.94, 4.95 and 4.92 g/cm^3 for samples A-D, respectively, achieving 94.9, 96.8, 97.1 and 96.5% of the theoretical density of 5.1 g/cm^3. Scanning electron microscopy (SEM) micrographs of sintered samples were recorded on a TESCAN electron microscope VEGA TS 5310MM device and are shown in Fig. 2. In all cases, sintering has reached the final stage showing a dense microstructure consisting of relatively large grains with closed porosity. Between these large grains, there are still some smaller ones. They are noticeable even in the samples obtained by sintering of the starting industrial powder (Fig. 2a).

Milling of the starting powder for 60 minutes combined with sintering has led to an overall reduction of the grain size and larger participation of smaller grains, but due to the agglomeration of the powder during milling larger crack like pores appear (Fig. 2b). Sieving of this powder eliminates larger agglomerates formed during milling, resulting in a microstructure with no large cracks consisting of large grains with closed porosity and smaller grains in between and some pores (Fig. 2c). Further milling in an agate mill for 24 hours followed by sieving through a 400 mesh resulted in a relatively homogeneous microstructure also with no large cracks, though some pores between grains remained (Fig. 2d). The average grain size and grain size distribution were determined from SEM images by averaging at least 200 grains from several SEM micrographs of the same sample using the SEMAPHORE software. The average grain size of the sample A (MZ-

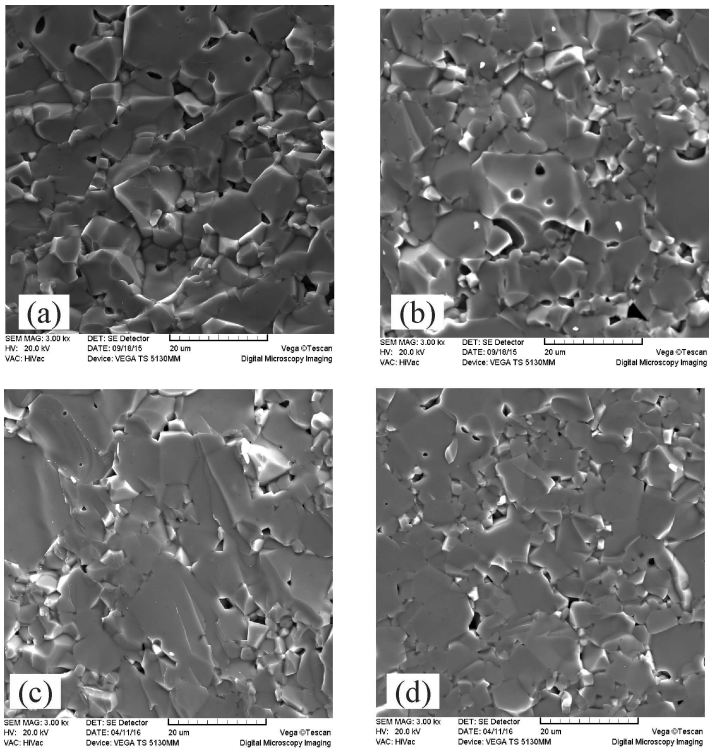

Figure 2. SEM micrographs of sintered samples fabricated using powders: a) MZ-0, b) MZ-1, c) MZ-1-325 and d) MZ-24-400

0) was determined as 6.62 μm with grains ranging between 1.92 and 20.2 μm. Milling of the starting powder reduced the average grain size to 5.51 μm determined for the sample B (MZ-1) with grains ranging between 0.78 and 27.7 μm. The sintered sample C, obtained from the sieved and milled powder (MZ-1-325) has similar value of the average grain size of 5.48 μm, but a slightly narrower grain size distribution. Similar value of the average grain size of 5.35 μm has the sample D, obtained from the powder MZ-24-400 (further milled in an agate mill followed by sieving).

3.2. *Complex permeability*

Complex permeability was measured in the frequency range from 0.1 MHz to 20 MHz at the magnetic flux density of 0.1 mT. The temperature of the CUTs was measured using a "TrueIR U5855A" thermal imaging camera from Keysight and it was in the range 26–28 °C. The real part μ' and the imaginary part μ'' of complex serial permeability of the sintered samples are shown in Fig. 3.

The real part of the complex permeability of the milled sample B ($\mu' = 270\,\mu_0$) is higher than that for the

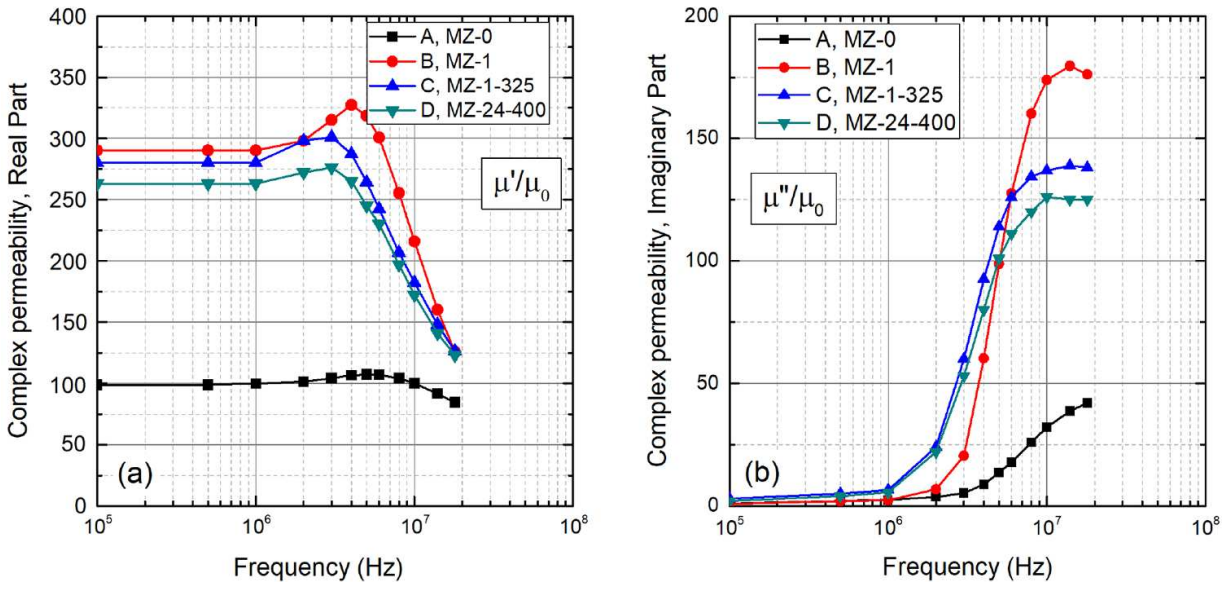

Figure 3. (a) Real and (b) imaginary part of the complex serial permeability as a function of frequency for sintered toroid samples A–D listed in Table 1

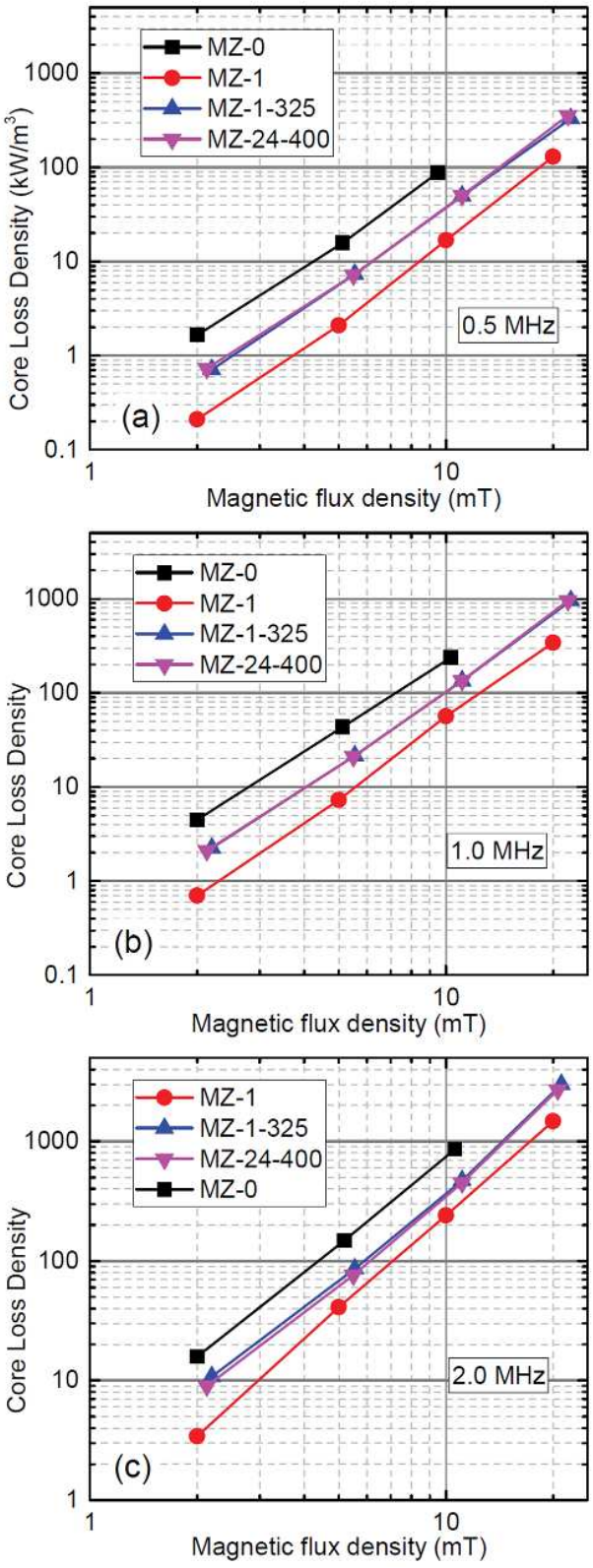

Figure 4. The Core loss density comparison of four different samples as function of peak flux density at frequency: a) 500 kHz, b) 1 MHz and c) 2 MHz

sample A ($\mu' = 100\,\mu_0$). The samples C and D, which are both milled and sieved, have μ' slightly different from the value obtained for the sample B. Additional milling and sieving of the sample D compared to the sample C resulted in slightly lower values of μ'. The μ' starts to decline at around 5 MHz for the sample B, and 3 MHz for the samples C and D, whereas μ' remains unchanged up to 10 MHz for the sample A. In the frequency range up to their cutoff frequencies the samples C and D have higher μ'' than the milled sample B.

3.3. Core loss density

The core loss density (CLD) was measured at four different values of the peak magnetic flux densities (2, 5, 10 and 20 mT) and at three frequencies (0.5, 1 and 2 MHz). The measurement results, shown in Fig. 4, compare CLD of all four samples at each of the three frequencies. Milling and sieving processes decreased the core loss density by a factor of 4 and 2, respectively.

Temperature of the surface of the CUT is measured using the thermal imaging camera. A period of 10 minutes between two successive measurements ensures the core is isothermal. The temperature is measured simultaneously with the CLD. Numerical values of the measured temperatures at frequencies 0.5, 1 and 2 MHz and the peak magnetic flux density, B_m at 20 mT are listed in Table 2. The sample B (prepared from the powder MZ-1) has the lowest temperature at each frequency, which is in correlation with the core loss density shown in Fig. 4.

Table 2. Temperature of the samples measured at peak magnetic flux density of 20 mT and three different frequencies

Sample (powder)	Temperature [°C]		
	0.5 MHz	1 MHz	2 MHz
A (MZ-0)	28	34	72
B (MZ-1)	28	33	60
C (MZ-1-325)	34	44	84
D (MZ-24-400)	36	49	82

The thermal images of the samples B (prepared from the milled powder) and C (prepared from the milled and sieved powder) at peak magnetic flux density of 20 mT and frequency 2 MHz are shown in Fig. 5. At the same frequency and magnetic flux density, the sample C reached a higher temperature compared to the sample B.

3.4. Hysteresis loop

Hysteresis loops for all samples were measured at the frequency of 10 kHz and temperature of 25 °C. To achieve high intensity of the magnetic field all four CUT were wound bifilar with $N = 50$ primary and secondary windings. Measured hysteresis loops of all four samples are shown in Fig. 6. Comparing the hysteresis loop of the sample A with others it can be concluded that milling and/or sieving process changes the hysteresis loop by increasing saturation and remanence magnetization. Milling can reduce the coercivity, while the coercivity of milled and sieved samples remains approximately the same as the one of the sample A (prepared from the starting powder MZ-0).

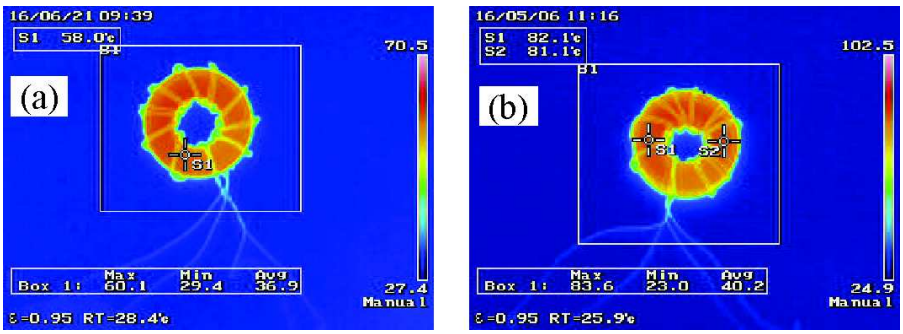

Figure 5. Thermal images at 20 mT and 2 MHz of: a) milled sample B and b) milled and sieved sample C

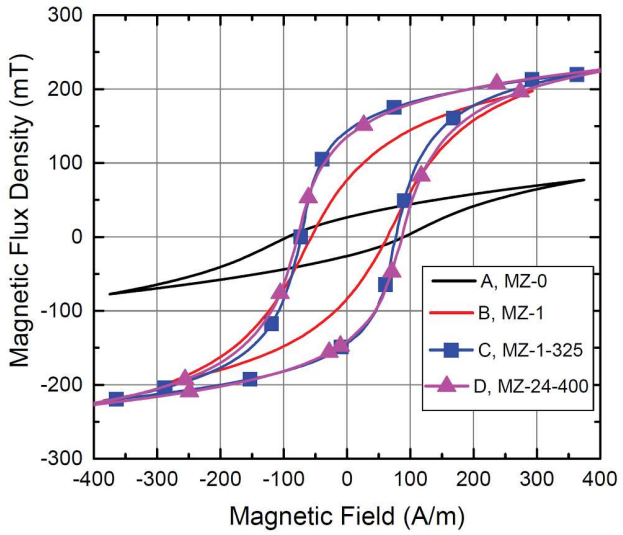

Figure 6. Hysteresis loop comparison of all four samples at 10 kHZ

IV. Modelling and simulations

The measurement data are used to fit the complex permeability versus frequency, CLD versus frequency and peak magnetic flux density, and static hysteresis loop at a single frequency and single peak magnetic flux density.

4.1. Modelling the complex permeability

In this paper, we propose two analytical functions for modelling the frequency dependence of the real and imaginary parts of complex permeability. This model is suitable for frequency characterization of the core in case of small sinusoidal excitation without DC bias when a linear relationship between magnetic field H and magnetic flux density B is achieved.

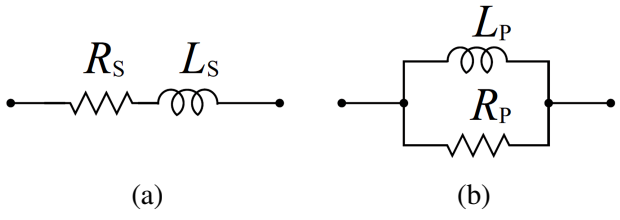

Figure 7. Circuit model for measuring complex permeability of lossy inductor

The complex permeability of ferrite cores can be modelled using serial or parallel presentations, as shown in Fig. 7. Serial presentation is common mainly because the serial complex permeability obtained from R_s and L_s is the one that is related to magnetic field H and magnetic flux density B:

$$H = \mu_s \cdot B = (\mu_s' - j\mu_s'')B \tag{1}$$

where μ_s' and μ_s'' are real and imaginary parts of serial complex permeability. Another reason is that serial complex permeability is the one that is obtained by measurements, as shown in Fig. 3. Instead of a serial presentation, in this paper the parallel presentation is used as a model that could be a direct representation of ferrite magnetic properties [12,13]. The conversion relations between serial and parallel elements are:

$$R_p = R_s(1+Q^2) \text{ and } L_p = L_s(1+Q^{-2}),\ Q = \frac{\omega \cdot L_s}{R_s} \tag{2}$$

$$R_s = \frac{R_p}{1+Q^2} \text{ and } L_s = \frac{L_p}{1+Q^{-2}},\ Q = \frac{R_p}{\omega \cdot L_p} \tag{3}$$

which yield the conversion relations between serial and parallel complex permeability:

$$\mu_p'' = \mu_s''(1+Q^2) \text{ and } \mu_p' = \mu_s'(1+Q^{-2}),\ Q = \frac{\mu_s'}{\mu_s''} \tag{4}$$

$$\mu_s'' = \frac{\mu_p}{1+Q^2} \text{ and } \mu_s' = \frac{\mu_p'}{1+Q^{-2}},\ Q = \frac{\mu_p'}{\mu_p''} \tag{5}$$

where μ_p' and μ_p'' are real and imaginary parts of parallel complex permeability.

Frequency behaviour of complex parallel permeability is modelled with analytical expression in the following form:

$$\mu_p' = \frac{\mu_{pi}'}{1+\left(\frac{f}{f_1}\right)^a},\ \mu_p'' = \frac{\mu_{pi}''}{1+\left(\frac{f}{f_2}\right)^b} \tag{6}$$

where f is the frequency, μ_{pi}' and μ_{pi}'' are initial values corresponding to μ_p' and μ_p'' at very low frequency, f_1 and f_2 are cut-off frequencies, a and b are slope factors.

Table 3. Complex permeability model coefficients and *R*-squared Goodness of Fit of the Imaginary part

Sample	μ'_{pi}/μ_0	f_1 [Hz]	a	μ''_{pi}/μ_0	f_2 [Hz]	b	R^2
A	100	2e8	2	7.0e3	0.9e6	1.40	0.9471
B	310	2e8	2	7.0e4	0.4e6	1.60	0.9103
C	300	2e8	2	4.5e4	0.4e6	1.55	0.9231
D	290	2e8	2	3.5e4	0.3e6	1.30	0.9694

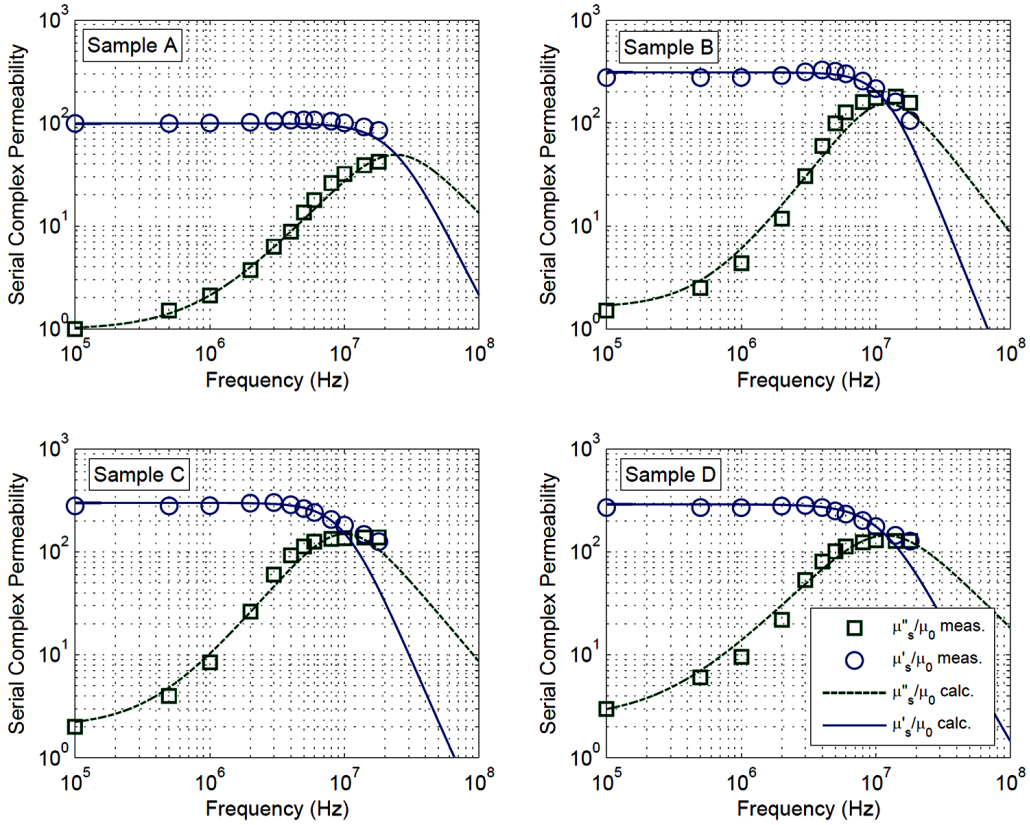

Figure 8. Calculated complex serial permeability of samples A, B, C and D using equation (6) and coefficients listed in Table 3 (solid lines present calculation while measured data are presented with markers)

The proposed model is based on the model already presented in literature [12,13] where two new coefficients, a and b are added. Coefficients obtained by fitting the model with the measured results for all four samples (A–D) are listed in Table 3.

Coefficients μ'_{pi} and μ''_{pi} are determined from values of complex serial permeability measured at a very low frequency using equation (4). The coefficient f_2 is near the frequency when μ''_p starts decreasing (μ''_s start increasing). The coefficient f_1 is beyond Snoek's limit (ferrite bandwidth, the frequency at which $Q = 1$) where μ'_p starts decreasing (μ'_s slows down its decrease). The coefficients f_1 and a describe the behaviour of complex permeability beyond Snoek's limit.

Measurement of complex permeability is performed in the frequency range up to about Snoek's limit. The complex permeability calculated using equations (5) and (6), shown in Fig. 8, are in good agreement with the measurements. Milling and sieving processes increase the permeability and decrease the ferrite bandwidth (f_2 of the samples B-D is less than for the sample A). The sample B has the highest b which means that losses increase more rapidly with increasing the frequency, but also has higher f_2 than the sample C and D. The sample B also has higher μ''_{pi} than the sample C and D which means that the sample B has lower core loss at low frequency (hysteresis loss). The coefficients f_1 and a describe the behaviour of complex permeability at frequencies beyond Snoek's limit and based on measured dataset they remain the same for all samples indicating that the ferrite bandwidth of analysed Mn-Zn material depends on how fast μ''_p decreases (how fast μ''_s increases).

Watson *et al.* [13] showed that in the case of low sinusoidal excitation without DC bias the CLD P_v could be calculated from the μ''_p and B_m using:

$$P_v = \pi \cdot f \frac{B_m^2}{\mu''_p} \tag{7}$$

where f is frequency, μ''_p is imaginary part of parallel complex permeability, and B_m is amplitude magnetic flux density at which the complex permeability is measured. The equation (7) and part of (6) with μ''_p, present

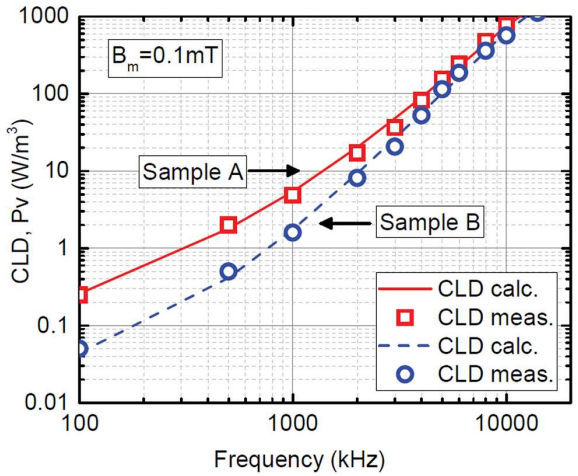

Figure 9. Calculated and measured CLD at B_m = 0.1 mT for samples A and B

the model of the CLD in small signal analysis. With the modified wattmeter method the complex permeability is measured simultaneously with the CLD and peak flux density B_m. The results of calculated and measured CLD for the samples A and B are shown in Fig. 9. The goodness of fit of the CLD model in small signal analysis was calculated for all four samples and listed in Table 4. The goodness listed in Table 4 is almost the same as the goodness of fit of the imaginary part of the complex permeability. The values of the R-squared goodness (very close to one) indicate that the model of the Mn-Zn core described with equation (6) could be used in small signal analysis to simulate the complex permeability as well as the core loss density using equations (6) and (7).

Table 4. R-squared Goodness of Fit of the CLD model at small signal

Sample	R^2
A	0.9980
B	0.9982
C	0.9986
D	0.9991

4.2. Modelling the core loss density

The CLD is modelled with the Steinmetz empirical equation [14] which is suitable for sinusoidal excitation without DC bias:

$$P_v = C_m \cdot f^{\alpha} \cdot B_m^{\beta} \tag{8}$$

where P_v is the CLD, f is frequency, B_m is the amplitude of magnetic flux density, C_m, α and β are coefficients obtained by fitting of measuring data. The coefficients are listed in Table 5 obtained by fitting the model with the measured results for all four samples A–D. The CLD is measured at four different frequencies 0.5, 1, 2 and 5 MHz, and four different values of the peak magnetic flux density 2, 5, 10 and 20 mT. The obtained coefficients, listed in Table 5, confirm the influence of milling and sieving on the core loss density. The sample B has the highest C_m, but the lowest α and β indicating the slowest increase of CLD with increasing frequency and magnetic flux density. Results of CLD calculation, using equation (8), are shown in Fig. 10. The simulation of the CLD at the 20 mT and 5 MHz shows that the sample B has the lowest CLD of about 10 MW/m^3 which is about 3 times less than the CLD of the sample A.

Table 5. CLD model coefficients and R-squared Goodness of Fit

Sample	C_m	α	β	R^2
A	0.1567	1.851	2.461	0.9989
B	1.121	1.658	2.422	0.9990
C	0.0316	1.961	2.601	0.9964
D	0.5894	1.853	2.953	0.9979

4.3. Modeling of hysteresis loop

Hysteresis models are mainly based on the Preisach model [15,16] or the Jiles-Atherton model [17–19]. These models have many coefficients that need to be determined which increase the calculation time and effort. We propose the model with three coefficients. This model can be used in the case of large signal sinusoidal excitation that leads to core saturation. In the first approach, the nonlinear behaviour law (B-H curve) of the ferrite material is modelled using:

$$B_{anh}(t) = B_s\left(\coth\frac{H(t)}{a} - \frac{a}{H(t)}\right) \tag{9}$$

which is based on the Jiles-Atherton modification of the Langevin equation. In equation (9) B_s is the saturation flux density, H is a magnetic field and a is a parameter with dimensions of the magnetic field which characterizes the influence of the anhysteretic magnetization. Using equation (9) anhysteretic magnetic flux density B_{anh} is modelled taking into account only the waveform modification by keeping B_{anh} in phase with the magnetic field.

Associated hysteresis loss is modelled introducing the time delay Δt between the magnetic field H and the magnetic flux density B_{anh}, by applying a convolution in the time domain:

$$B(t) = \int_{-\infty}^{\infty} B_{anh}(\tau)\cdot\delta(t-\Delta t-\tau)\mathrm{d}\tau = B_{anh}(t-\Delta t) \tag{10}$$

where Δt is a coefficient obtained by fitting with measured data. The coefficients obtained by fitting the model with the measured results for all four samples A–D are listed in Table 6. Instead of Δt, a coefficient $\Delta\varphi = 2\Delta t/T$ is listed in Table 6, where T is the period of the waveforms. Figure 11 compares the measured and calculated B-H curves for all four samples A–D at frequency of 10 kHz. Milling increased the saturation about two times, while additional sieving did not introduce significant improvement.

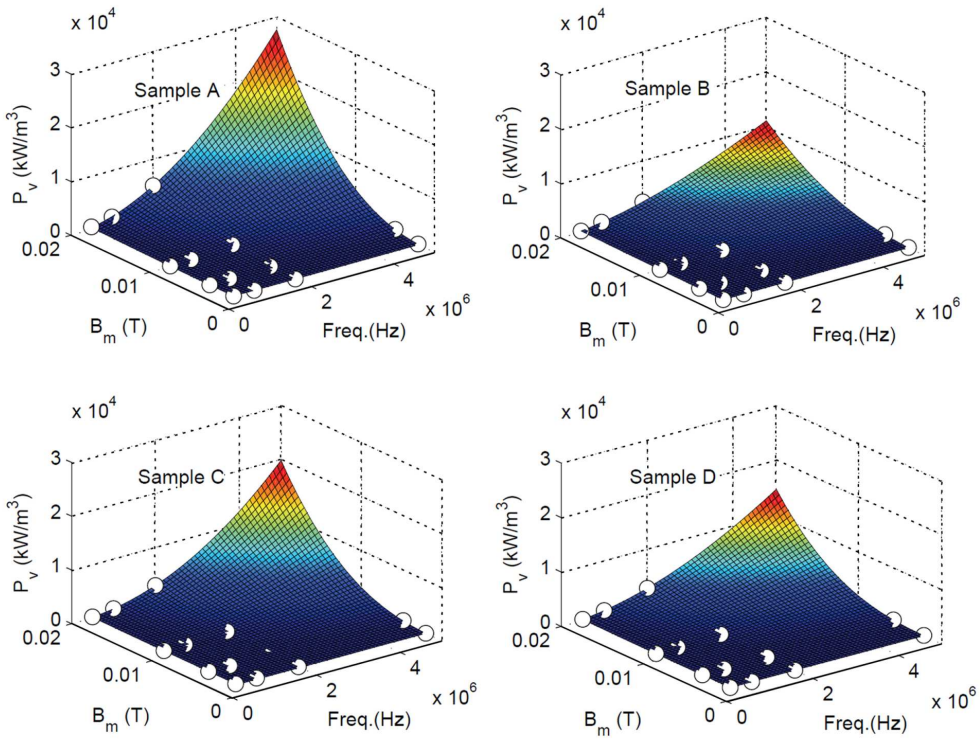

Figure 10. Calculated CLD of samples A, B, C, and D using equation (7) and coefficients from Table 4 with prediction of the CLD at 5 MHz and 20 mT (circles indicate measured values)

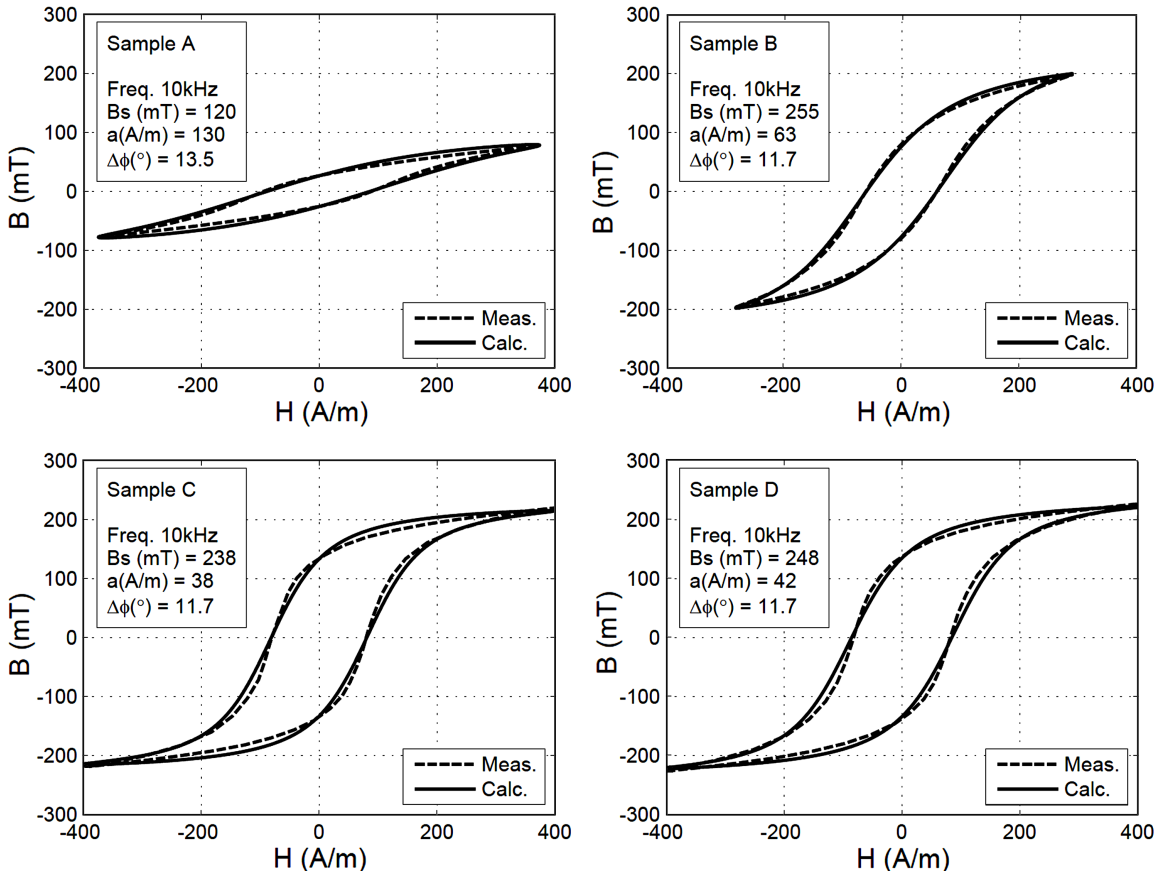

Figure 11. Simulated hysteresis loop of samples B and C using equation (9) and coefficients from Table 5

V. Discussion

The estimated empirical parameters described in this section are not correlated directly with material structure, but they are in relation with the resistivity, permittivity and permeability of the used ferrite material, which depend on structure characteristic and sintering temperature.

The sample B has μ' that is 2.7 times higher and a cutoff frequency that is 2 times lower than that of the sample A. However, in the frequency range up to 2 MHz both samples A and B have the same imaginary part of relative complex permeability. These results show that the milling process increases the relative permeability and decreases the cutoff frequency. Observing the CLD, shown in Fig. 4, we find that the core loss density of the sample B is 4 and 6 times lower than that of the sample A, measured at 1 MHz and 0.5 MHz, respectively. The milling process can significantly reduce the core loss density. Comparing the hysteresis loops, the sample B has higher saturation and remanence than the sample A, while the coercivity of the sample B is less than that of the sample A, as shown in Fig. 6. The remanence of the milled sample B is 4 times higher than that of the sample A. Overall conclusion is that the milling process can significantly improve magnetic properties. Milling changes the sample microstructure and this is reflected in changes of the magnetic properties. Milling changes the sample microstructure by reducing the grain size, but longer milling can result in powder agglomeration, so it is necessary to determine the optimal milling time. In our previous work [10] we analysed the influence of different milling times on changes in electric properties and determined 60 minutes as optimal.

In addition, in comparison to the milling process the influence of the combined processes (milling and sieving) on magnetic properties is not particularly significant, though sieving eliminated the largest agglomerates and a microstructure with fewer cracks was obtained. Observation of these results leads to the conclusion that additional milling in an agate mill followed by sieving through a 400 mesh did not improve any analysed properties, so it does not need to be applied.

VI. Conclusions

In this paper, the influence of starting powder milling and sieving on the magnetic properties of Mn-Zn ferrite was investigated. The influence was analysed by comparing the obtained microstructure, relative permeability, core loss density and hysteresis loop of four toroidal shaped samples sintered at 1200 °C for 2 h. Relative permeability, core loss density and hysteresis loop measurements were performed using the watt-meter method. The experimental results show significant improvement with milling and improved microstructure with less large cracks when the additionally milled powder was sieved. Relative permeability is increased about 3 times. Core loss density is reduced four times by milling of the starting powder. Milling of the starting powder increases saturation and remanence while decreases coercivity.

Magnetic properties of the analysed samples are additionally calculated applying appropriate models. The coefficients of used models are calculated by fitting the experimental results. The core loss density is modelled with the Steinmetz empirical equation, while two new proposed models are used for the complex permeability and hysteresis loop. The real and imaginary parts of the complex permeability, as well as the hysteresis loop, are all modelled with three coefficients simplifying the fitting procedures. Measured and calculated results are in good agreement. The obtained results confirm the influence of milling on magnetic properties of the analysed Mn-Zn material.

Acknowledgements: This work was supported by the Serbian Ministry of Education, Science and Technological Development under the grant for the projects TR32055 and TR32016.

References

1. H. Waqas, A.H. Qureshi, K. Subhan, M. Shahzad, "Nanograin Mn-Zn ferrite smart cores to miniaturize electronic devices", *Ceram. Int.*, **38** (2012) 1235–1240.
2. H. Su, H. Zhang, X. Tang, X. We, "Effects of calcining and sintering paremeters on the magnetic properties of high-permeability MnZn ferrites", *IEEE Trans. Magn.*, **41** [11] (2005) 4225–4228.
3. P.J. van der Zaag, J.J.M. Ruigrok, A. Noordmeer, M.H.W.M. van Delden, P.T. Por, M.Th. Rekveldt, D.M. Donnet, J.N. Chapman, "The initial permeability of polycrystalline MnZn ferrites: The influence of domain and microstructure", *J. App. Phys.*, **64** (1993) 4085–4095.
4. G. Ott, J. Wrba, R. Lucke, "Recent developments of Mn-Zn ferrites for high permeability applications", *J. Magn. Magn. Mater.*, **254** (2003) 535–537.
5. H.N. Ji, Z.W. Lan, Z.Y. Xu, H.W. Zhang, J.X. Yu, M.Q. Li, "Effects of second milling time on temperature dependence and improved Steinmetz parameters of low loss MnZn power ferrites", *IEEE Trans. Appl. Superconduct.*, **24** [50] (2014) 1–4.
6. K. Zehani, B. Ahmadi, V. Loyau, Y. Champion, L. Bessais, M. LoBue, E. Labouré, F. Mazaleyrat, "Structural, dielectric, and magnetic properties of NiZnCu ferrites synthesized by reactive spark plasma sintering process", *IEEE Trans. Magn.*, **50** [4] (2014) 1–4.
7. Y. Matsuo, K. Ono, T. Hashimoto, F. Nakao, "Magnetic properties and mechanical strength of MnZn ferrite", *IEEE Trans. Magn.*, **37** [4] (2001) 2369–2372.
8. N. Blaz, A. Maric, I. Atassi, G. Radosavljevic, Lj. Zivanov, H. Homolka, W. Smetana, "Complex permeability changes of ferritic LTCC samples with variation of sintering temperatures", *IEEE Trans. Magn.*, **48** [4] (2012) 1563–1566.
9. Y. Han, G. Cheung, A. Li, C.R. Sullivan, D.J. Perreault, "Evaluation of magnetic materials for very high frequency power applications," pp. 4270–4276 in *IEEE Power Electron. Specialists Conf.*, https://doi.org/10.1109/PESC.2008.4592628, Rhodes, Greece, 2008.

10. M. Milutinov, M.V. Nikolic, M. Lukovic, N. Blaz, Z. Vasiljevic, Lj. Zivanov, O. Aleksic, "Influence of starting powder milling on structural properties, complex impedance, electrical conductivity and permeability of Mn-Zn ferrite", *J. Mater. Sci.: Mater. Electron.*, **27** (2016) 11856–11865.
11. M. Milutinov, N. Blaz, Lj. Zivanov, "Ferrite core loss measurement issues and technique", *Proceedings of 18th International Symposium on Power Electronics, EE 2015*, https://doi.org/10.13140/RG.2.1.3546.3123, Novi Sad, Serbia, 2015,.
12. J.K. Watson, S. Amoni, "A four-component model for high- ferrites", *IEEE Trans. Magn.*, **25** [5] (1989) 4227–4229.
13. J.K. Watson, S. Amoni, "Using parallel complex permeability for ferrite characterization", *IEEE Trans. Magn.*, **25** [5] (1989) 4224–4226.
14. J.E. Brittain, "A steinmetz contribution to the AC power revolution", *Proc. IEEE*, **72** (1984) 196–197.
15. F. Preisach, "Über die Magnetische Nachwirkung", *Zeitschrift für Physik*, **94** (1935) 277–302.
16. H.Y. Lu, J.G. Zhu, S.Y.R. Hui, "Measurement and modeling of thermal effects on magnetic hysteresis of soft ferrites", *IEEE Trans. Magn.*, **43** [11] (2007) 3952–3960.
17. D.C. Jiles, J.B. Thoelke, M.K. Devine, "Numerical determination of hysteresis parameters the modeling of magnetic properties using the theory of ferromagnetic hysteresis", *IEEE Trans. Magn.*, **28** [1] (1992) 27–35.
18. N. Schmidt, H. Guldner, "A simple method to determine dynamic hysteresis loops of soft magnetic materials", *IEEE Trans. Magn.*, **32** [2] (1996) 489–496.
19. L. D'Alessandro, A. Ferrero, "A method for the determination of the parameters of the hysteresis model of magnetic materials", *IEEE Trans. Instrum. Meas.*, **43** [4] (1994) 599–605.